International Journal of Hydrogen Energy 103 (2025) 576–588

Contents lists available at ScienceDirect

International Journal of Hydrogen Energy

journal homepage: www.elsevier.com/locate/he

Enhanced performance of platinum coated titanium bipolar plates for proton exchange membrane water electrolyzer under diverse pH and temperature conditions

Yingyu Ding [a], Xiejing Luo [a], Luqi Chang [a], Xiang Li [b], Wei Han [b], Chaofang Dong [a,*]

[a] Beijing Advanced Innovation Center for Materials Genome Engineering, Key Laboratory for Corrosion and Protection (MOE), Institute for Advanced Materials and Technology, University of Science and Technology Beijing, Beijing, 100083, China
[b] China Iron and Steel Research Institute Group, Beijing, 100081, China

ARTICLE INFO

Handling Editor: Dr V Palma

Keywords:
PEMWE
Bipolar plates
Conductivity
pH and temperatures

ABSTRACT

As renewable hydrogen energy serves for primary input of cyclic clean energy systems, environmental instability and fluctuations during energy conversion impose multiple challenges to the stable and efficient operation of proton exchange membrane water electrolyzer (PEMWE) cells. Herein, the performance and stability of platinum coated titanium (Pt/Ti) bipolar plates to withstand diverse environmental conditions (H_2SO_4 pH = 1, 3, 5 at 60, 70 and 80 °C) and relatively high electrolysis potentials (0.6–1.8 $V_{Ag/AgCl}$) were explored. The thickness of platinum coating was about 680 nm without obvious defects, which reduced the corrosion current density of Pt/Ti bipolar plates to 0.09 μA cm^{-2} in a simulated PEMWE environment with applied potential of 1.0 $V_{Ag/AgCl}$ for 10 h. Meanwhile, the value of interfacial contact resistance (ICR) of the Pt/Ti bipolar plates was measured as 1.5 mΩ cm^2, showing no significant increase in high-level potentials tests under diverse environment. In addition, the influence of internal and external conditions to the electrolyzer stack on bipolar plates were discussed in detail, and the interrelated effects of pH values and applied potentials on the corrosion resistance of the Pt/Ti bipolar plates were established, especially in the range around the value of the water electrolysis potential.

1. Introduction

Hydrogen energy, recognized as one of the most promising clean energy sources of the 21st century, has reached a preliminary industrial scale. However, it still confronts numerous vital technological challenges that demand breakthroughs. Among these challenges, hydrogen production, a crucial and forefront section within the hydrogen application system, remains an area that requires substantial research investment. PEMWE systems, are currently the primary strategy for hydrogen generation at present with their flexible start-stop responses, high energy conversion efficiency, cleanliness, and adaptability to fluctuating energy sources [1–4].

Within the PEMWE systems, bipolar plates serve as a crucial component, providing mechanical support along with heat and electrical conductivity. They are foundational not only to the application performance of the entire stack but also represent considerable account of the cost considerations (initial production, surface protection, and failure) of the electrolysis [5,6]. According to recent reports [7–9], the operating conditions inside the electrolyzer generally fall within the approximate ranges of pH = 2–4, 60–80 °C, and 1.6–2.0 V $_{RHE}$. Considering cost and performance concerns, metal bipolar plates are recognized for their superior mechanical properties, ease of fabrication, and cost-effectiveness compared to graphite and composite counterparts which were widely employed in proton exchange membrane fuel cells (PEMFCs) with lower voltage service conditions [10–13]. Among the metal bipolar plates, stainless steel and titanium are the most extensively researched materials. Stainless steel plates are more cost-effective, while struggle to meet performance requirements in the electrolytic environment so that typically employed under low-electric-potential conditions in PEMFCs [7,14–16]. Titanium, on the other hand, exhibits commendable corrosion resistance, enabling its long-term use in corrosive electrolytic environments [8,9]. However, titanium plates face challenges due to the poor conductivity of the titanium dioxide passivation layer formed on their surface, leading to reduced electrolysis efficiency [17–22]. Therefore, ensuring the performance stability of bipolar plates is crucial for securing a long-term, affordable hydrogen

* Corresponding author.
E-mail address: cfdong@ustb.edu.cn (C. Dong).

https://doi.org/10.1016/j.ijhydene.2025.01.211
Received 1 August 2024; Received in revised form 15 November 2024; Accepted 13 January 2025

supply. The inherent susceptibility of metal bipolar plates to corrode, which reduces their service life and leads to failure, underscores the importance of appropriate surface modification as the most effective method to enhance their application performance for long-term stability [23–26]. Current work results on various coatings deposited on titanium bipolar plates were listed in Table 1, including noble metal, metal compounds (nitride/carbide/oxide), carbon-based and organic coatings, have demonstrated promising application prospect on titanium bipolar plates [27–31]. Jung et al. [32] coated titanium with Au by a sputtering method to prevent the oxidation of titanium. Li et al. [33] deposited three different metal nitride (Ta/TaN, Cr/CrN and Nb/NbN) composite coatings on the surface of titanium bipolar plates by magnetron sputtering. They found that Cr/CrN possessed the best anti-corrosion capability. However, during the test, the coating had poor adhesion and was prone to detach from the substrate. And the polarization resistance (R_p) of the uncoated Ti substrate was significantly improved from 119 Ω cm^2 to 4765 Ω cm^2 and 374 Ω cm^2 with Ta/TaN and Nb/NbN coatings, respectively. Chen et al. [34] applied a TiCr transition layer to improve the corrosion resistance and surface conductivity of TiCrN coating. The current density and ICR value of double-layer TiCr/TiCrN were decreased to 0.25 μA/cm^2 and 6.5 mΩ cm^2, respectively. Moreover, the introduction of composite coatings further ensures structural integrity under electric potential conditions, which typically require a corrosion resistant base layer and a conductive top layer [18,35–37].

For titanium bipolar plates, more suitable for high electric potential electrolytic environments, the coatings not only need to mitigate corrosion failures during service but also address the insulating nature of the passivized titanium surface. As shown in Fig. 1, there has been a lot

Table 1
Various research works of coated titanium bipolar plates.

Preparation method	Coatings	Test conditions	i_{corr} (μA·cm^{-2})	*ICR* (mΩ·cm^2)	$i_{+0.6V}$ (μA·cm^{-2})	Thickness (μm)	Ref
Multi-arc ion plating	C/(Ti:C)/Ti	pH = 3 H_2SO_4, 0.1 ppm HF, 80 °C	0.027	1.51	9.53	0.31	[38]
Electrophoretic deposition, thermal treatment	TiN–C	0.5 M H_2SO_4, 5 mg L^{-1} F^-, 80 °C	1.410	7.50	–	–	[39]
High power impulse magnetron sputtering	TiN	0.5 M H_2SO_4, 2 ppm HF, 70 °C	0.106	3.51	0.28	0.49, 0.67, 0.73, 1.09	[40]
Double cathode glow discharge plasma	TaCN	0.5 M H_2SO_4, 0/3/6 ppm HF 70 °C	0.032	9.61	0.11	16.50	[41]
High power impulse magnetron sputtering	CrN	pH = 3 H_2SO_4, 0.1 ppm HF, 80 °C	–	6.82	0.08	–	[26]
Hybrid powder reduction	Ti_4O_7	0.1 M H_2SO_4, 2 ppm F 70 °C	0.063	7.61	–	5.00	[42]
Double cathode sputtering	TiZrHfMoW	0.5 M H_2SO_4, 1/3/5 ppm HF 75 °C	0.021	20.30	0.88	25.00	[43]
Hydrothermal and impregnation	C-PTFE/GS-CNT	0.5 M H_2SO_4, 2 ppm HF 70 °C	0.014	0.28	0.05	–	[35]
Magnetron sputtering technology, vacuum heat treatment	C/TiC	0.5 M H_2SO_4, 5 ppm HF, 80 °C	0.740	2.34	–	0.048	[44]
Cathodic arc evaporation physical vapor deposition	(Ti,Zr)N	0.5 M H_2SO_4, 3 ppm HF, 60 °C	0.212	0.64	–	3.30	[45]
Electrochemical metallizing	Au–TiO2	0.5 M H_2SO_4, 2 ppm F^-, room temprtature	0.013	2.70	–	–	[46]
Multi-arc ion plating	TiCr/TiCrN	0.5 M H_2SO_4, 2 ppm HF, 80 °C	0.105	3.22	–	2.60	[34]
Physical vapor deposition magnetron sputtering	Pt	pH = 3 H_2SO_4, 2 ppm NaF, 80 °C	0.761	4.12	–	0.68, 1.02, 3.38	[47]
Arc ion plating	Ti–Ag–N	0.5 M H_2SO_4, 2 ppm F^- 70 °C	0.650	2.30	–	1.50	[48]
Plasma surface modification plasma alloying furnace	NbC	0.5 M H_2SO_4, 3 ppm F^- 75 °C	–	16.60	0.32	0.70	[49]
Pulsed bias arc ion plating	Au	0.5 M H_2SO_4, 1 ppm HF, 80 °C	0.005	4.60	0.03	0.05	[50]
Unbalanced magnetron sputtering	a-C	pH = 3 H_2SO_4, 0.1 ppm HF, 80 °C	0.920	20.00	–	0.76	[51]
High power pulsed magnetron sputtering	a-C: H/TiC	0.5 M H_2SO_4, 5×10^{-6} M F^- 70 °C	0.980	1.60	–	2.55, 2.40	[52]

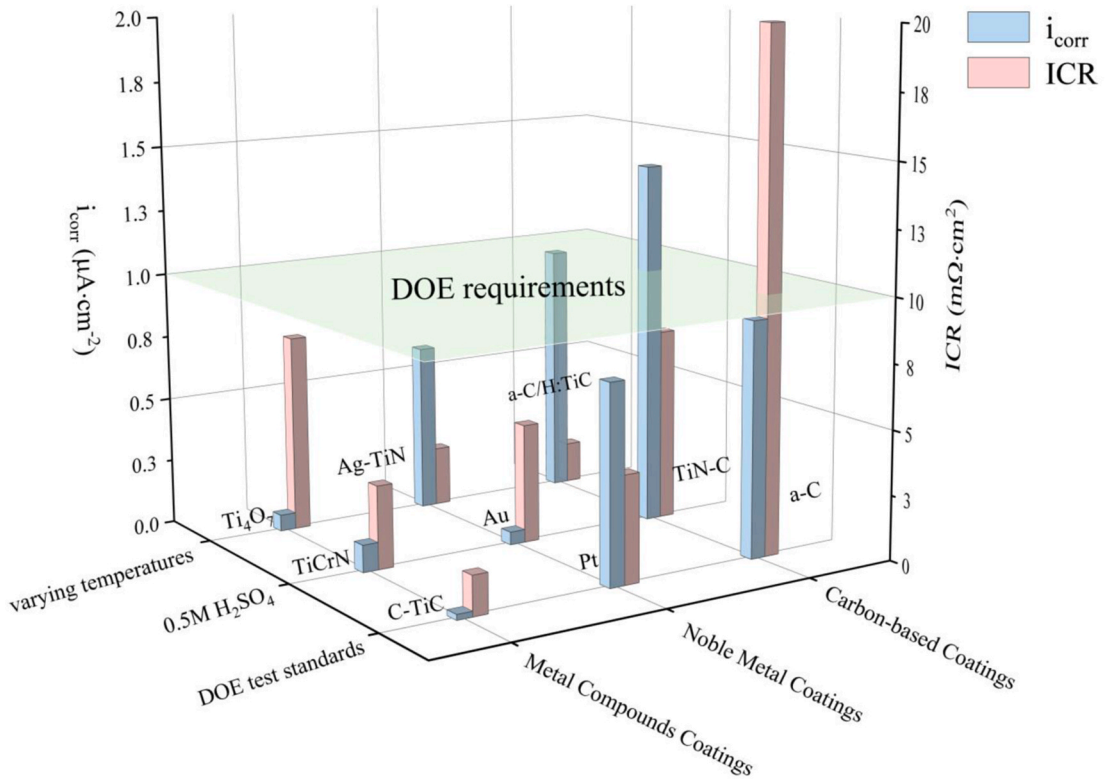

Fig. 1. Comparison on performance of various coatings applied on titanium bipolar plates.

of research progress in metal composite coatings in recent years, while lack of long-term durability evaluation [34,38,39,42,47,48,50–53]. Researchers have found that carbon-based coatings could effectively protect the substrates from corrosion in a low cost and great efforts have been made by element doping on structural characteristics and applying multilayer a-C films [54–56]. Zhang et al. [57] constructed LaB_6-doped carbon films by magnetron sputtering ion plating and Ying et al. [52] prepared (a-C: H/TiC)/(TiCN)/(TiN) multilayer films by high power pulsed magnetron sputtering (HiPIMS) technology. As reported, the sp hybrid orbitals have a decisive role in conductivity and corrosion resistance on carbon-based coatings and limits a balance on the ratio of the two factors, which needs a second or third party to make up for the shortcomings in one certain aspect. Above on these findings, platinum, with its excellent conductivity and status as a noble metal, exhibits strong stability and, has been proven to be a feasible protective coating for bipolar plates [24,38,58]. And the application of a platinum coating over a titanium-protected stainless steel substrate has achieved cell performance comparable to the baseline [59,60].

The impact of water electrolysis operating conditions on the corrosion of metal bipolar plates holds significant relevance. Dynamic changes in voltage load and start-stop operations not only exceed the degradation of the membrane electrode assembly (MEA) but also affect the corrosion behavior of metal bipolar plates due to abnormal potential imposition [61–63]. Within the actual application of generating hydrogen through water electrolysis, not only the issues arising from fluctuating energy inputs that are prominent but the internal solution environment of the electrolysis operation, alongside external conditions, is subject to variation as well [29,64]. The actual pH value and temperatures of electrolyte are fluctuated in a range of 2–5 and 60–80 °C as reported, respectively [51,65,66]. However, current research exhibits a lack of assessment regarding the service stability of coated bipolar plates and their resilience against environmental fluctuations. In our work, an analysis on the long-term service stability of Pt/Ti bipolar plates under diverse water electrolysis conditions was conducted, including examinations on the service stability of the Pt coating in simulated PEMWE environments under high-level voltage conditions, as well as the changes in the overall conductive performance of the coated plates. Furthermore, the impact of diverse temperature and pH value working conditions on the corrosion resistance and conductive performance of the coated plates was evaluated as well.

2. Materials and methods

2.1. Microstructure and composition characterization

Pure titanium plates (TA1) with the size of 1.5 cm × 1.5 cm × 2 mm were served as the samples and substrates, initially subjected to surface refinement protocol involving abrasion with sandpaper, ultrasonic purification, and subsequent desiccation to facilitate the application of a platinum layer. The Pt coatings were deposited through the magnetron sputter system equipped with platinum target (99.9% purity), and the chamber was vacuumed before deposition process. Pt coating was deposited on the surface of Ti substrates after cleaning by etching it with the argon ions to remove surface oxide layer.

The investigatory focus extends to a comprehensive examination of the surface morphology and crystalline architecture of the specimens, utilizing X-ray Diffraction (XRD) scanned as 8°/min in range of 10–90°, Scanning Electron Microscopy (ZEISS Gemini SEM 300, Germany), Focus Ion Beam (FIB; Helios G4 PFIB) and the finer Transmission Electron Microscopy (TEM; JEOL JEM-F200) system equipped with energy dispersive X-ray spectrometry (EDS) and XPS (Thermo Scientific ESCALAB 250Xi, USA).

2.2. Interfacial contact resistance measurements

Comparative analyses of the conductivity between pure and Pt/Ti bipolar plates were undertaken using interfacial contact resistance measurements through typical method [67], elucidating the conductivity variances of post-operational durations under diverse conditions with vertical resistivity tester (SI-ONE) Commercial carbon paper

(TGP-H-060) was used to simulate common gas diffusion layers (GDLs). These investigations were conducted within a pressure range of 0.2–3.0 MPa, with test adjustments of 0.2 MPa.

2.3. Electrochemical tests

The electrochemical behavior of each specimen was elucidated through a series of electrochemical evaluations conducted with O_2 bubbled in a Corrtest electrochemical workstation, which provided insights into the open-circuit potential (OCP), potentiostatic and potentiodynamic polarization characteristics, and electrochemical impedance spectroscopy (EIS). For the electrochemical assessments, a three-electrode configuration was adopted, composed of an Ag/AgCl reference electrode, a Pt counter electrode, and the Pt/Ti specimen as working electrode.

Initial measurements commenced with the determination of the OCP lasted over a span of 30 min under diverse conditions. EIS tests were performed both before and after 4 h potentiostatic polarization (pH = 1, 3, 5 H_2SO_4, 60, 70 and 80 °C), capturing data across a frequency spectrum ranging from 10 mHz to 100 kHz with a 10 mV amplitude. The impedance profiles, reflective of the properties in varied environments and after certain operational durations, were analytically fitted using Zview software, facilitating the generation of Nyquist and Bode diagrams. The dynamic range for potentiodynamic scanning polarization in simulated PEMWE environment (pH = 3 H_2SO_4, 80 °C) was delineated from - 0.25 V (vs. OCP) to 2.2 $V_{Ag/AgCl}$, executed at a scanning rate of 1 mV s^{-1}. And the 4 h potentiostatic polarization scheme was adopted at 0.6, 1.2 and 1.8 $V_{Ag/AgCl}$ for investigation on the response of Pt/Ti bipolar plates under variable pH and temperature conditions. Furthermore, potentiostatic polarization experiments were conducted at 0.6, 0.8, 1.0, 1.2, 1.4, 1.6 and 1.8 $V_{Ag/AgCl}$ in simulated PEMWE environment (pH = 3 H_2SO_4, 80 °C), monitoring the current density for 10 h to research effect of electric voltage conditions.

3. Results and discussion

3.1. Microstructure and composition

The XRD spectra of the prepared Pt/Ti bipolar plates are illustrated in Fig. 2(a). The detected diffraction peaks primarily originate from the surface coating of Pt (PDF#01-087-0642), indicating the excellent uniformity and density on the electrode surface of prepared Pt coating which can provide effective safeguard for titanium substrates from degradation caused by corrosive ions. Further, reflections from the Pt (111) plane on the electrode surface were significantly stronger than those from other planes, implying a preferential growth orientation of the film along the (111) plane direction.

Fig. 2(b) presents the XPS spectra of Pt4f, including $4f_{7/2}$ and $4f_{5/2}$, which can be specifically divided into three component peaks, corresponding to three metal states. Peaks at binding energies of 70.98 eV and 74.28 eV were attributed to the $4f_{7/2}$ and $4f_{5/2}$, respectively. More specific, the peaks at 74.18 eV and 70.88 eV account for metallic state of Pt (0), peaks at 74.68 eV and 71.28 eV correspond to Pt (II), while those at 75.98 eV and 72.48 eV represent state of Pt (IV). From the spectra results, the majority of Pt atoms were stabilized at Pt (0) metallic state, indicating a refined Pt coating was prepared on Ti substrate.

In Fig. 3(a), the morphology of platinum coating deposited on the Ti substrate and element distribution on the plate surface are shown in micron scale. The surface structure of the prepared Pt coating was uniform and dense, covering Ti substrate to support enhancement of anti-corrosion and conductivity with no obvious microscopic defects. Further zooming on the details revealed that the surface of the platinum coating was composed of densely packed nanoscale fine particles. From the cross-sectional morphology and mapping results obtained by FIB-TEM characterization shown in Fig. 3(b) and (c), the obvious integrated substrate with uniform coating structure can be observed, contributed to characterizing the coating thickness which is approximately 680 nm. Besides, the ideal interface combination between Ti substrate and Pt coating has been confirmed according to the high-resolution morphology in Fig. 3(b_3) as no obvious gap demarcation could be observed.

3.2. Interfacial contact resistance

The ICR served as a quintessential indicator of the conductive property of electrode coatings. Decrease in the ICR value signified an intensified conductivity of the coating under regulated pressure, which can enhance the hydrogen production efficiency within water electrolysis systems. In practical PEMWE stack, the traditional operation pressure in range of 0.1–1.6 MPa had been increased up to over 3.0 MPa for efficient hydrogen storage and transportation [62,68,69]. Here, a pressure range of 0.2–3.0 MPa was selected for the ICR testing to assess the electrical conductivity of the bipolar plates more accurately under practical application conditions. As depicted in Fig. 4(a), conductivity of bare and platinum coated samples was measured following the regulate method [70,71]. Two sheets of carbon paper were placed between the

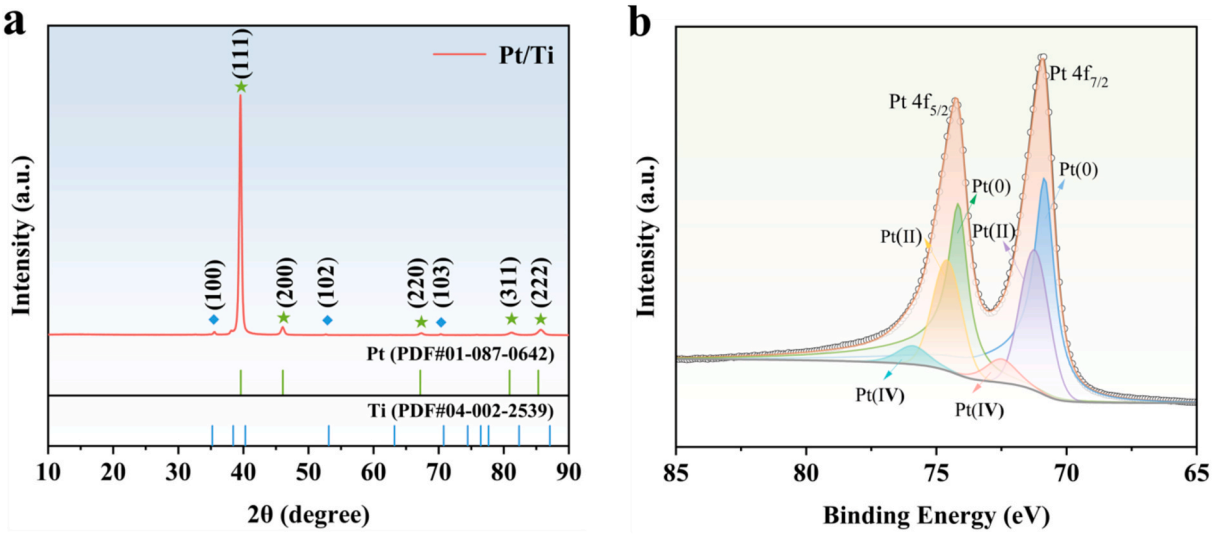

Fig. 2. (a) XRD patterns and (b) XPS spectra of Pt 4f for Pt/Ti samples.

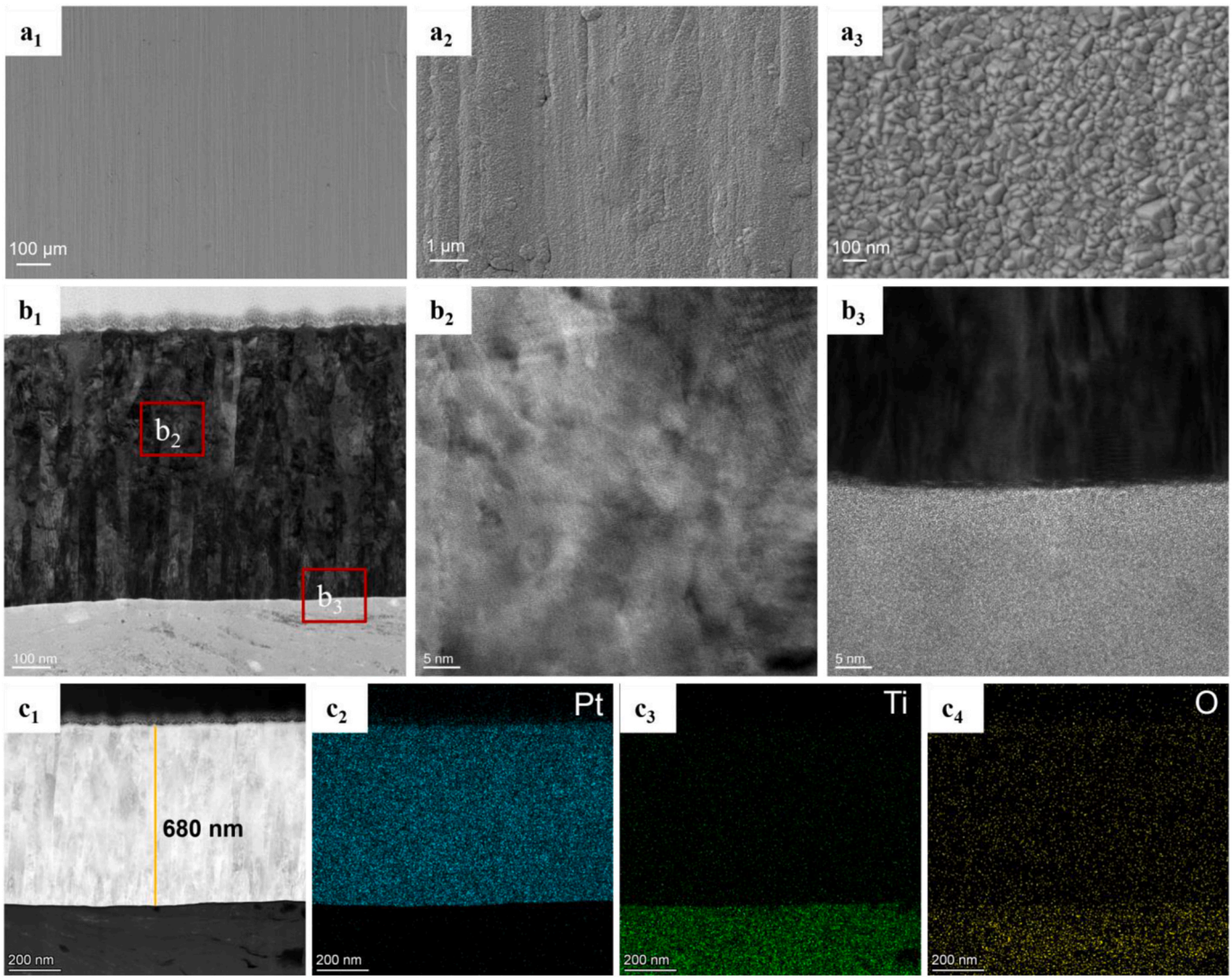

Fig. 3. (a) SEM characterization and (b) Cross-sectional FIB-TEM morphology and the corresponding (c) element mapping of Pt/Ti samples.

two gold-plated copper electrodes, and the sample was sandwiched in the structure. The actual measurement device was showed in Fig. 4(b). Under the simulation of external pressure, the resistance between the two electrodes was measured in real time, then the contact resistance of the sample interface was calculated by the formular:

$$ICR = S \times (R_1 - R_2) / 2 \quad (3\text{-}1)$$

where S is the contact area of the test samples, R_1 and R_2 represent the resistance of carbon paper with and without Pt/Ti specimens, respectively. The ICR value of uncoated and Pt coated titanium samples before long-term potentiostatic polarization were measured and the results were shown in Fig. 4(c) and (d). With a gradual increment in compaction force from 0.2 MPa to 3.0 MPa, the ICR of titanium electrodes sharply declined from an initial 160.9 mΩ cm^2, eventually stabilized around 20 mΩ cm^2. At a pressure of 1.4 MPa, the ICR value for the uncoated titanium electrodes was recorded at 29.6 mΩ cm^2; conversely, the incorporation of a platinum coating introduced a reduction in the ICR value to 1.5 mΩ cm^2, marking a 94.9% decrease at 1.4 MPa.

3.3. Electrochemical tests

3.3.1. Electrochemical impedance spectroscopy

Electrochemical impedance spectroscopy data was obtained by collecting electrochemical feedback signals under the action of perturbation to characterize the surface state of platinum-coated electrodes in solutions under different temperatures and pH conditions both before and after 4 h of potentiostatic testing at specific voltages. The equivalent circuit used is embedded in Fig. 5(a), where R_s was the equivalent resistance of the solution, the R_f represented the resistance of the surface film layer of the Ti substrate and R_{ct} indicated the resistance of the charge transfer reaction. In addition, the introduced constant phase elements CPE_f and CPE_{dl} and the corresponding deviation parameters n_1 and n_2 to describe the film capacitance (C_f) between the substrate and the solution and the double-layer capacitance (C_{dl}) of the coating, respectively. Combining the fitting data such as surface resistance and charge transfer resistance, it was found that the platinum coating has the ability to improve the corrosion resistance of the bipolar plates under various test conditions. A higher R_{ct} value indicates that the platinum coating protects the plate surface and prevents damage caused by corrosive ions. In addition, the corrosion resistance of platinum-coated electrode plate samples changed regularly depending on the test conditions.

The Nyquist plot gave the metal corrosion behavior based on the capacitor semicircle radius. On the one hand, as the pH value decreased or the temperature increased, the capacitor arc radius noticeably decreased from Fig. 5, implying a negative change in metal corrosion resistance. On the other hand, the arc radius of the sample after potentiostatic polarization decreased by a large extent, which displayed

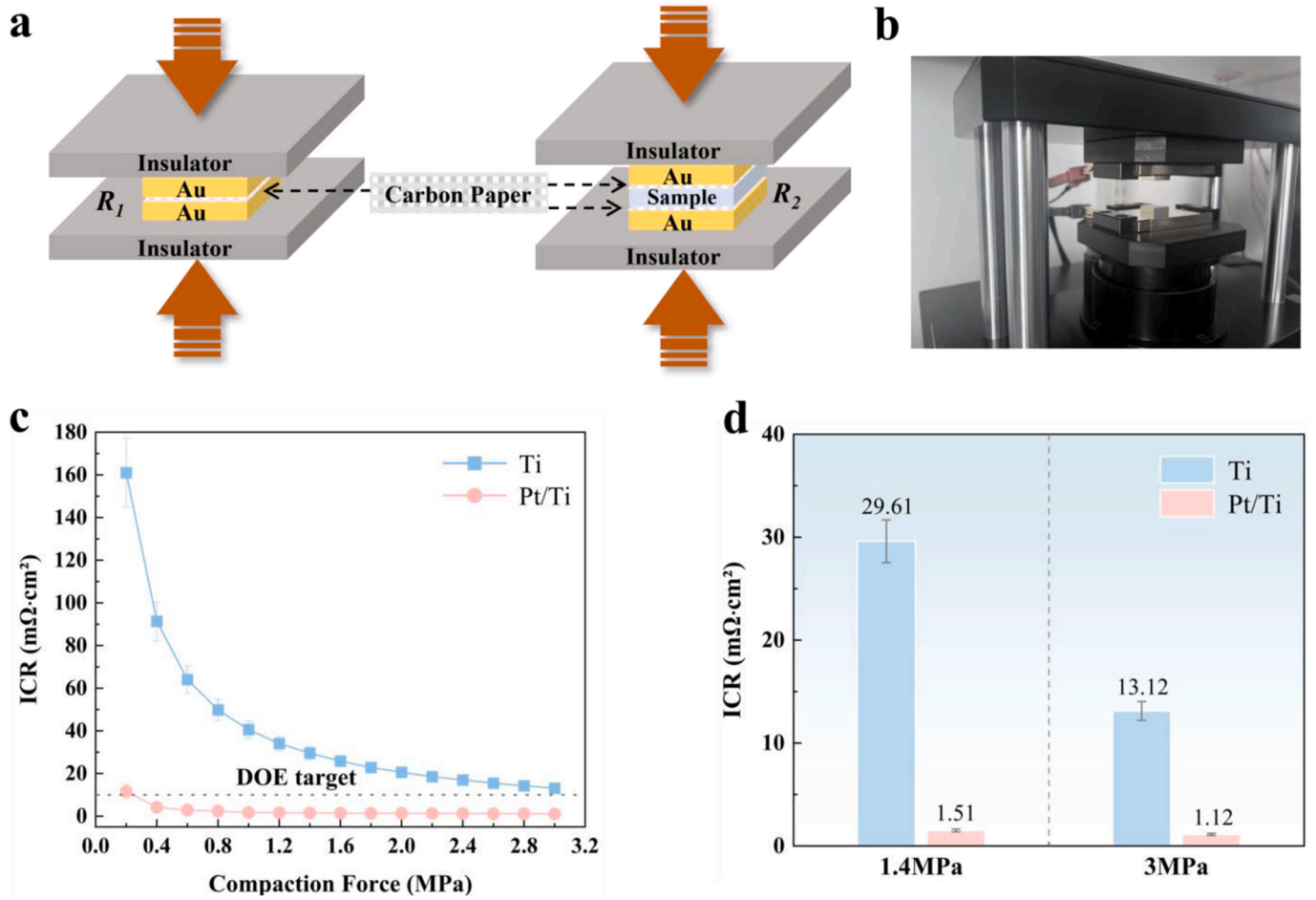

Fig. 4. ICR of (a) schematic diagram; (b) equipment illustration (c) bare Ti and Pt/Ti samples with carbon papers; (d) comparison of bare Ti and Pt/Ti at 1.4 MPa and 3.0 MPa.

that the surface of the electrode plate would be more susceptible to corrosion and dissolution due to the increase of service voltage. The Bode diagram showed the interfacial contact characteristics between the solution and the metallic platinum coating. In the high frequency region of Bode diagram, it represents the resistance between the electrolyte solution and the working electrode, the medium frequency region describes the change process of the surface film layer, and the low frequency region illustrates the corrosion of the plate base. Therefore, the impedance mode value in the low-frequency region is positively related to the protective effect of the coating on the electrode plate. As the acidity of the test solution increased from pH = 5 to 1, the impedance mode values of the samples were tested before applying the voltage of 0.6 $V_{Ag/AgCl}$ for 4 h, experienced a drop by about 1 order of magnitude value. Similarly, as the temperature increased to 80 °C, the modulus values of the samples decreased in a certain extent in almost every test environment.

In the operating environment of PEMWE, the electrochemical reactions occurring on the platinum coating can primarily be categorized into two types: the dissolution of metal ions and the formation of oxides. These three reactions are described by the following equations:

$$Pt \rightarrow Pt^{2+} + 2e^{-} \ (E_0 = 1.188\ V_{RHE}) \quad (3\text{-}2)$$

$$Pt + H_2O \rightarrow PtO + 2H^{+} + 2e^{-} \ (E_0 = 0.980\ V_{RHE}) \quad (3\text{-}3)$$

$$Pt + 2H_2O \rightarrow PtO_2 + 4H^{+} + 4e^{-} \ (E_0 = 0.837\ V_{RHE}) \quad (3\text{-}4)$$

Many studies have corroborated on these reactions, given the standard potential of redox process as E_0, and one report linked the increased proportion of O^{2-} on the surface of the platinum coating to its reduced corrosion resistance [72,73]. According to our experimental results, as both the pH of the solution decreased and the temperature increased, the harshness of the environment intensified. In response, the values of R_f and R_{ct} generally exhibited a decreasing trend, indicating that the surface state of the platinum coating undergone changes, which in turn diminished its protective effect on the substrate. This observation is consistent with the trends depicted in the Nyquist plot.

Further examination can be obtained from the impedance fitting data given in Table 2, it is apparent that as the temperature increased from 60 °C to 70 °C and 80 °C, both R_f and R_{ct} values decreased, signifying a reduction in the corrosion resistance of the membrane as well as an enhancement in electron transfer reactions. As the pH decreased, indicating increased acidity in the solution, R_f continued to decrease. However, the R_{ct} value initially decreased in a pH = 3 solution but showed a slight increase when the pH dropped further to 1. This suggested that the corrosion resistance of the membrane follows a pattern consistent with both acidity and temperature variations. The electron transfer reactions, however, exhibited a more systematic change within a certain pH range, with a reverse enhancement as the acidity of the solution continuously rose beyond a certain threshold.

3.3.2. *Potentiodynamic polarization*

The potentiodynamic scanning tests were used to evaluate the electrochemical corrosion behavior of the bipolar plates. By fitting the polarization curve in the Tafel interval, the corrosion potential (E_{corr}) and current density (i_{corr}) were mainly obtained, as well as the current density at 0.6 $V_{Ag/AgCl}$ ($i_{+\ 0.6\ V}$), as shown in Table 3. Compared with bare titanium plates, the corrosion resistance of titanium plates modified

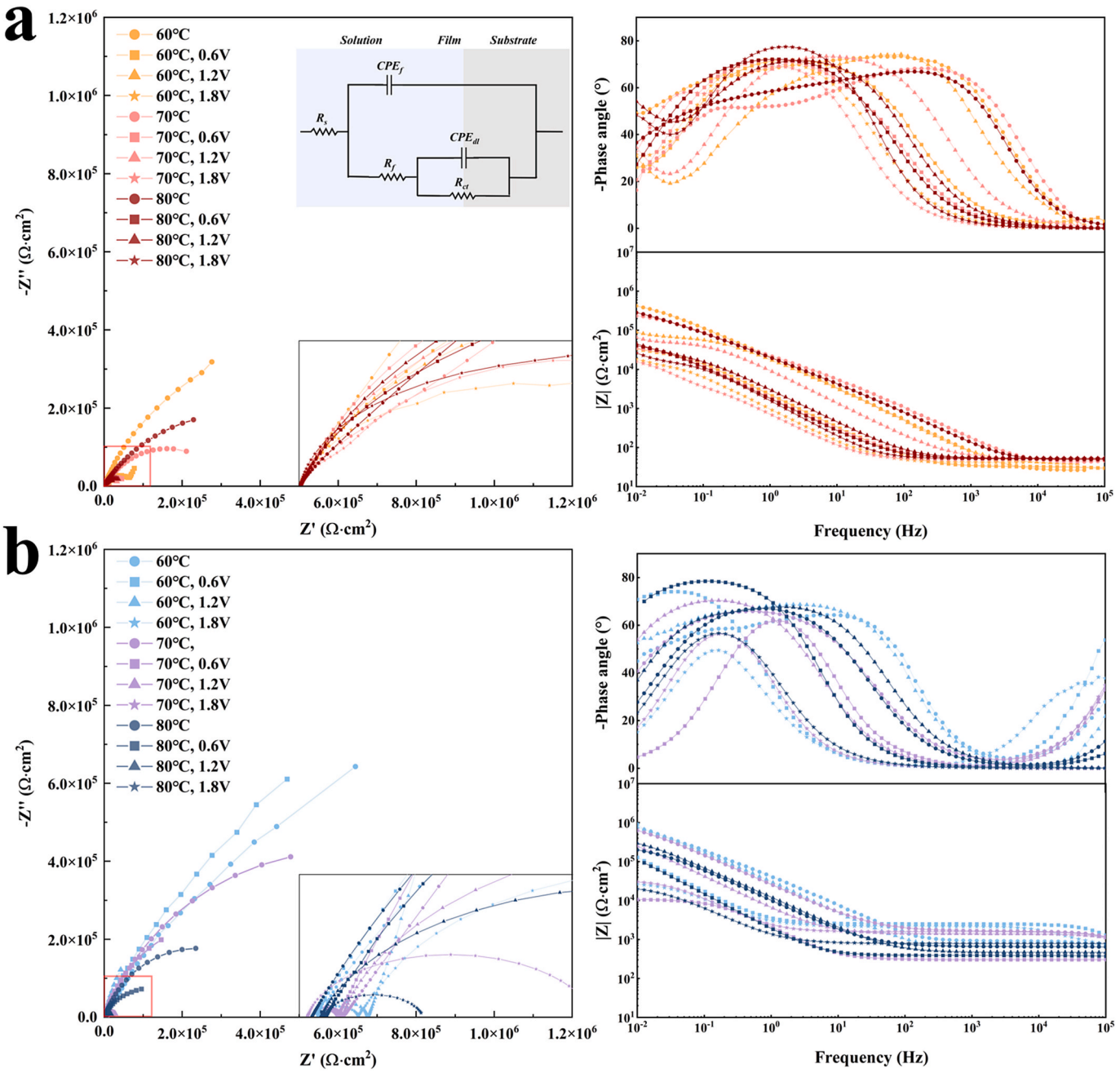

Fig. 5. Nyquist and Bode plots in EIS measurements before and after 4 h potentiostatic polarization in H_2SO_4 electrolyte (a) pH = 1 and the equivalent circuit model (b) pH = 3 (c) pH = 5 at 60, 70 and 80 °C.

with a platinum coating was significantly improved. As shown in Fig. 6, the corrosion resistance was significantly increased with positive shift of E_{corr}, and the corrosion current density was reduced as well. showed an obvious enlargement account The E_{corr} of the Pt/Ti bipolar plate increased with a decrease in pH value, among which the corrosion current density was relatively consistent under the test conditions of pH = 3, 5. It is worth noting that in the highly acidic pH = 1 solution, there was an obvious slope decrease in the curve near 1.2 $V_{Ag/AgCl}$, resulting in a higher corrosion current density value near 1.4 $V_{Ag/AgCl}$ which was significantly higher than the other two groups. This may be attributed to passivation on the surface of platinum metal under more acidic conditions. Besides, current density of catalysis in water electrolysis process got empty calculated. On the other hand, raise of temperature caused an increase in corrosion current density, implying that higher temperature conditions would reduce the corrosion resistance of the coated plates.

3.3.3. *Potentiostatic polarization for 4 h*

Aiming to explore the impact of test environment changes on the durability of the plates, 3 certain polarization potentials of 0.6 $V_{Ag/AgCl}$, 1.2 $V_{Ag/AgCl}$, and 1.8 $V_{Ag/AgCl}$ were applied to the samples under different test conditions (pH = 1, 3, 5 H_2SO_4, 60, 70 and 80 °C) for 4 h. Related results have been displayed in Fig. 7, the current density decreased rapidly in the initial stage after applying the potential and then remained stable. As the potential increased, the stable current density value after 4 h of polarization leveled up as well. For 0.6 $V_{Ag/AgCl}$ and 1.2 $V_{Ag/AgCl}$, the modified Ti plates had better durability, and a more stable corrosion current density which was at the micro-ampere level, then current density got increased as the applied potential was raised to

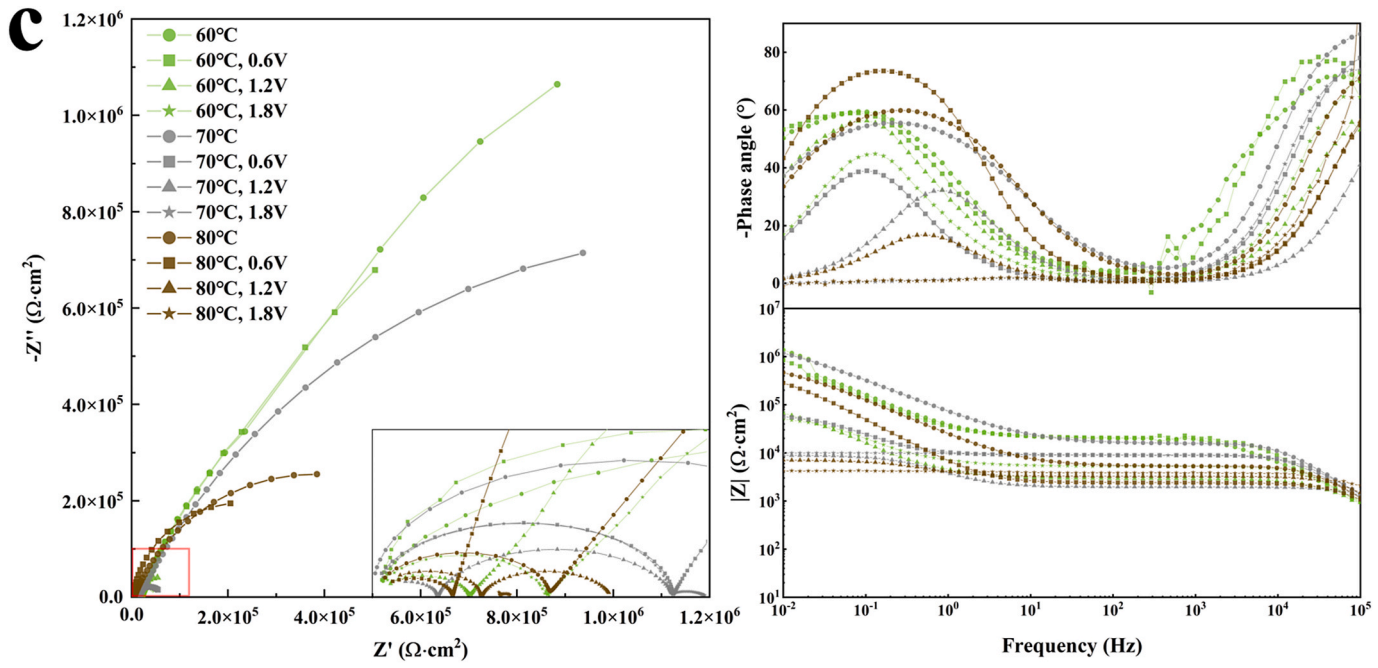

Fig. 5. (*continued*).

Table 2
Electrochemical impedance parameters for Pt/Ti samples before potentiostatic polarization in H_2SO_4 electrolyte (pH = 1, 3, 5 at 60, 70 and 80 °C).

Temperature (°C)	pH	R_s (Ω·cm²)	R_f (Ω·cm²)	R_{ct} (Ω·cm²)	C_f ($\Omega^{-1}cm^{-2}s^n$)	n_1	C_{dl} ($\Omega^{-1}cm^{-2}s^n$)	n_2
60	1	25.93	664.4	1.57E6	4.39E-6	0.91	8.08E-6	0.63
	3	274.7	548.9	1.51E6	3.78E-10	0.84	6.63E-6	0.75
	5	373.74	2.06E4	2.73E6	9.84E-9	0.87	8.13E-6	0.84
70	1	41.97	9.97E3	3.13E5	3.81E-6	0.85	1.04E-5	0.65
	3	249.3	4.01E4	1.63E5	9.36E-6	0.82	3.31E-6	0.71
	5	301.3	2.63E4	2.38E6	8.01E-10	0.93	4.02E-6	0.73
80	1	49.22	8.02E3	6.78E5	7.27E-7	0.87	1.41E-5	0.63
	3	101.3	5.53E4	2.65E5	4.02E-10	0.71	2.27E-5	0.80
	5	149.5	7.14E4	7.49E5	1.20E-9	0.79	1.08E-5	0.76

Table 3
Polarization parameters of the Pt/Ti samples in H_2SO_4 electrolyte (pH = 1, 3, 5) at 60, 70 and 80 °C.

	Temperature (°C)	pH	E_{corr} ($V_{Ag/AgCl}$)	i_{corr} (μA·cm⁻²)	$i_{+0.6V}$ (μA·cm⁻²)
Pt/Ti	60	1	0.5815	0.5485	0.1883
		3	0.5276	0.1324	0.2579
		5	0.3821	0.0356	0.2493
	70	1	0.5877	0.1232	0.0234
		3	0.5221	0.0635	0.1680
		5	0.4027	0.0382	0.4539
	80	1	0.6034	0.0770	−0.0127
		3	0.5188	0.1604	0.4247
		5	0.4033	0.0446	0.3876
Ti	60	1	−0.0483	9.1249	13.2274
		3	0.0457	0.5140	6.9007
		5	−0.0691	1.4056	5.4467
	70	1	−0.1597	25.7253	14.1217
		3	−0.2231	2.8873	5.5836
		5	0.0933	0.2041	4.5871
	80	1	−0.1228	32.2615	17.7892
		3	0.0443	0.3943	6.0467
		5	0.1252	3.2514	5.4165

1.8 $V_{Ag/AgCl}$.

Among them, under the voltage conditions of 0.6 $V_{Ag/AgCl}$ and 1.8 $V_{Ag/AgCl}$, as the pH value of the solution decreased, the corrosion current density showed an increasing trend, implying that corrosion reactions were more likely to occur on the surface of the electrode plate in an acidic environment. However, at a potential of 1.2 $V_{Ag/AgCl}$, the corrosion current density increased as the pH value of the solution raised as depicted in Fig. 7(b) due to the combined influence of pH and polarization potential. Considering the voltage of 1.2 $V_{Ag/AgCl}$ is close to the theoretical water decomposition voltage, and the closer the pH value is to 7, that is, when the solution is approximately close to a pure water environment, the greater degree of water decomposition reaction, the more similar corrosion current density pattern. Under the high voltage condition of 1.8 $V_{Ag/AgCl}$ where water decomposition could fully proceed, the corrosion current density resumed the law of increasing as the pH value of the solution decreased as Table 4. These findings highlight the importance of considering environmental factors, such as voltage fluctuations and pH variations, which may lead to the degradation of electrode performance in practical applications. By incorporating reaction kinetics and E-pH (Pourbaix) diagrams, it is crucial to identify the optimal working conditions for coated electrodes and prevent performance deterioration due to environmental fluctuations.

Therefore, under this test scheme, the increasement of the acidity of the solution had a negative impact on the plate corrosion. The degree of reaction had been obviously deepened, especially under the test condition of pH = 1, the corrosion current density value was about 2 orders of magnitude higher than that of other test groups. It can be seen that the pH value of the solution had a significant impact on the service stability of the plate. Under the same pH and potential test conditions, the corrosion current density of the plate under the 80 °C test environment

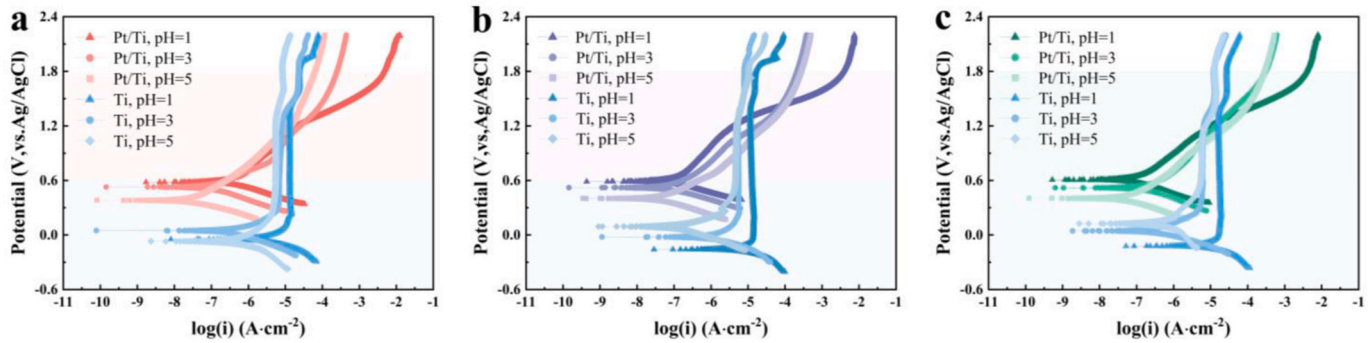

Fig. 6. Potentiodynamic polarization curves of Pt/Ti and Ti samples in H_2SO_4 (pH = 1, 3, 5) at (a) 60 °C (b) 70 °C (c) 80 °C.

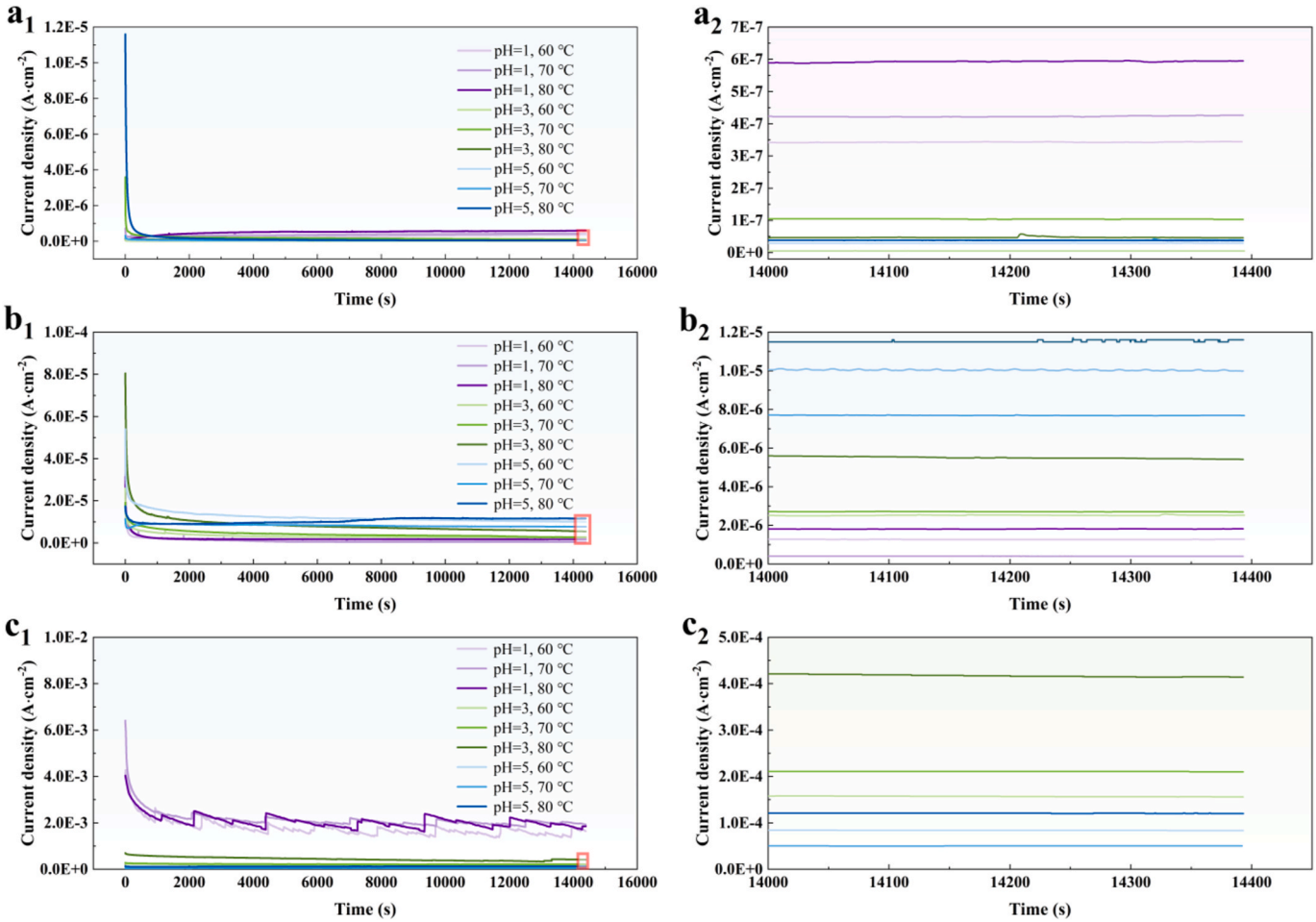

Fig. 7. Potentiostatic polarization curves of Pt/Ti at (a_1, a_2) 0.6 $V_{Ag/AgCl}$, (b_1, b_2) 1.2 $V_{Ag/AgCl}$, (c_1, c_2) 1.8 $V_{Ag/AgCl}$ for 4 h in varying electrolytes with different pH and temperatures.

was greater than that of 60 and 70 °C. Illustrating that thermal conditions had subtle influence in the corrosion current density under different test conditions. And temperature increase could aggravate the surface corrosion reaction and water electrolysis reaction under more acidic and higher potential test conditions.

3.3.4. *Potentiostatic polarization for 10 h*

The pure titanium plate was subjected to potentioststic polarization of 0.6, 0.8, 1.0, 1.2, 1.4, 1.6 and 1.8 $V_{Ag/AgCl}$ for 10 h in a test environment of pH = 3, 80 °C. Due to the existence of surface titanium dioxide, the current density showed a very small value under various conditions, even at a high voltage of 1.8 $V_{Ag/AgCl}$, confirmed the fact poor conductivity of titanium in PEMWE electrolyte. With potentials applied over time, the obtained curves in Fig. 8 all exhibited rapid current density drop in the initial period and then stabilized due to the presence of protective oxide layers. According to the results of potentiostatic polarization tests for Pt/Ti samples in Fig. 9, it is evident that at potentials below the water decomposition threshold, the corrosion current density of platinum-coated titanium samples was consistently lower than that of uncoated across all measured potentials. For instance, at 1.0 V, the corrosion current density of the coated electrode decreased from 0.17 to 0.09 μA cm^{-2}, reflecting a reduction of approximately 47.1%.

As shown in Table 5, all the values of current density were <10 μA

Table 4
Current density of the Pt/Ti samples after 4 h potentiostatic polarization in varying electrolytes with different potentials, pH and temperatures.

Temperature (°C)	pH	$i_{+0.6V}$ (μA·cm^{-2})	$i_{+1.2V}$ (μA·cm^{-2})	$i_{+1.8V}$ (μA·cm^{-2})
60	1	0.3441	1.2745	1392.8227 - 1819.8762
	3	0.0047	2.5284	155.9613
	5	0.0293	9.9862	83.4946
70	1	0.4261	0.3954	1824.4322 - 2131.4761
	3	0.1031	2.6918	210.3561
	5	0.0391	7.6824	50.3742
80	1	0.5951	1.8204	1727.1145 - 2248.3602
	3	0.0458	4.4231	414.2531
	5	0.0372	11.5659	120.3065

cm^{-2} at voltage conditions of 0.6, 0.8, 1.0 and 1.2 $V_{Ag/AgCl}$ and the corrosion current density values were relatively close at 0.6, 0.8, and 1.0 $V_{Ag/AgCl}$, while there was a significant increase at 1.2 $V_{Ag/AgCl}$. Firstly, combining the potentiodynamic polarization curve in Fig. 7, when the potential is scanned to about 1.0 $V_{Ag/AgCl}$, a turning point appeared in the polarization curve of the sample, with the slope of the curve and corrosion resistance of the coating decreased. Secondly, when the conditions for water decomposition voltage are confirmed which is 1.23 V_{SHE}, there is a certain degree of water electrolysis on the surface of the plate. As reported, platinum group metal are regarded as standard catalysts for the oxygen evolution reaction (OER) in PEMWEs owing to their excellent catalytic effect, which caused increase in current densities [74,75]. The corrosion current densities of the plates under voltage conditions of 1.4, 1.6 and 1.8 $V_{Ag/AgCl}$ were much higher than that of 0.6–1.2$V_{Ag/AgCl}$ as recorded in Fig. 9 and Table 5. Moreover, from the trend of corrosion current density changing with test time, it can be seen

Table 5
Current density of the Pt/Ti samples after 10 h potentiostatic polarization applied with different potential.

Sample and electrolyte	Potential ($V_{Ag/AgCl}$)	Current density (μA·cm^{-2})
Pt/Ti (pH = 3, H_2SO_4, 80 °C)	0.6	0.0127
	0.8	0.0730
	1.0	0.0957
	1.2	3.2163
	1.4	82.0186
	1.6	295.0761
	1.8	562.2433 - 991.3102

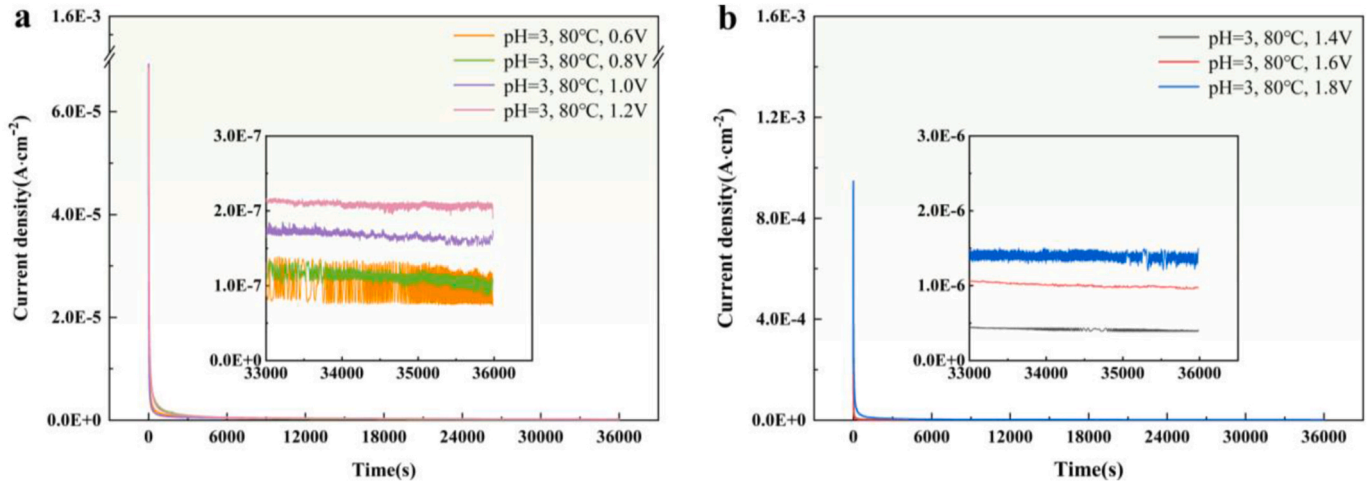

Fig. 8. Potentiostatic polarization curves of bare Ti samples after 10 h potentiostatic polarization at (a) 0.6–1.2 $V_{Ag/AgCl}$ and (b) 1.4–1.8 $V_{Ag/AgCl}$ in H_2SO_4 (pH = 3, 80 °C).

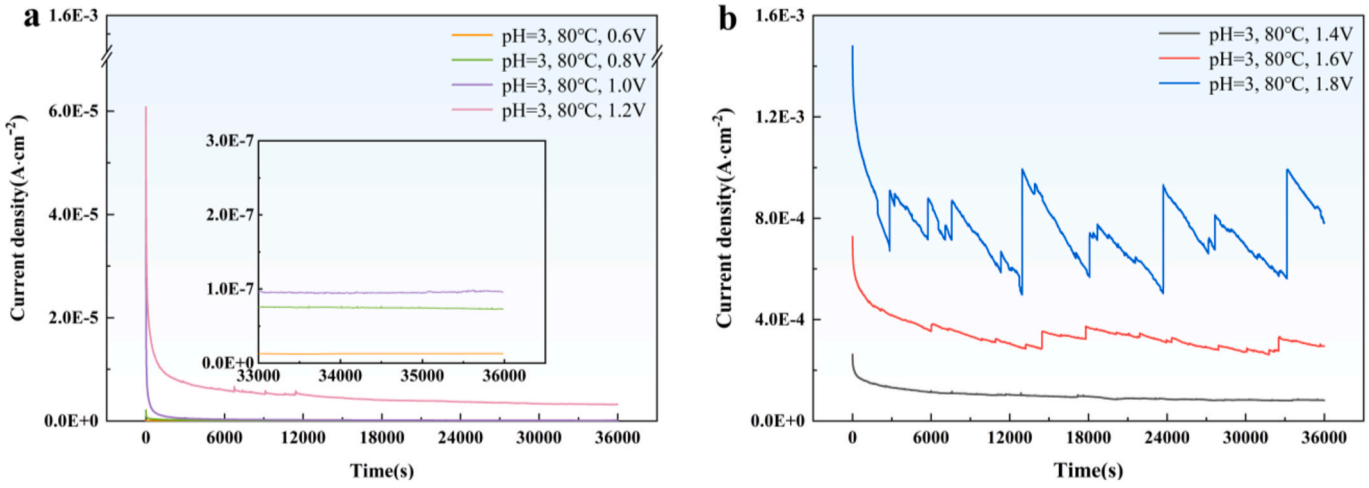

Fig. 9. Potentiostatic polarization curves of Pt/Ti samples after 10 h potentiostatic polarization at (a) 0.6–1.2 $V_{Ag/AgCl}$ and (b) 1.4–1.8 $V_{Ag/AgCl}$ in H_2SO_4 (pH = 3, 80 °C).

that under the potential condition of 1.8 $V_{Ag/AgCl}$, there are obvious differences in the surface reaction of the plates, causing fluctuations in current density, which do not exist under other test potential conditions.

Comparing the surface morphology of the samples after 10 h potentiostatic polarization tested at different potentials, it can be found that the coating maintained its integrity under the test conditions of 0.6–1.0 $V_{Ag/AgCl}$, and there was no obvious change in the particles at the nanoscale. When the voltage increased to 1.4 $V_{Ag/AgCl}$, the surface integrity of the coating got slight jeopardized and the nano-particles on the coating surface aggregated to clusters with its number further increased with voltage rose.

As shown in Fig. 10(f, g), surface morphology revealed a noticeable increase in coating roughness after the polarization at 1.6 and 1.8 $V_{Ag/AgCl}$, causing a reduction in smoothness and uniformity. However, at higher magnifications, the coating retained a commendable degree of overall homogeneity, despite slight particle aggregation in the size of 500–800 nm induced by elevated voltages. Notably, no significant defects were observed in Fig. 10(h, i), which suggested that the platinum coating exhibited robust durability under high potential conditions, effectively acted as a barrier to prevent corrosive ions from penetrating and compromising the substrate. The prepared nano-thick platinum coating can maintain relative structural integrity at a voltage of up to 1.2 $V_{Ag/AgCl}$, which was sufficient for water decomposition, and showed ideal corrosion resistance and stability in an electrolytic water hydrogen production environment. Increasing the voltage to high-level extent would cause a subtle degree of damage to the coating, forming slight aggregation of nanoparticles on the surface.

3.3.5. Interfacial contact resistance after 10 h polarization

A critical metric in evaluating the efficacy of coatings, especially for titanium electrodes covered by an oxide layer impeding conductivity, is its potential to positively influence electrical conduction. Hence, the ICR of Pt/Ti bipolar plates after exposure to electrolysis potentials over 10 h were thoroughly measured as shown in Fig. 11, increased from 1.51 Ω cm^2 to 1.59 Ω cm^2, 3.69 Ω cm^2 and 4.62 Ω cm^2 applied with 0.6, 1.2 and 1.8 $V_{Ag/AgCl}$, respectively. Given the superior conductivity of platinum, aqueous electrolysis conditions exerted a negligible effect on altering the conductive capacity of the coating. After 10 h of operation, the escalation in testing voltage from 0.6 to 1.2 and 1.8 $V_{Ag/AgCl}$ revealed a prominent increase in ICR values with higher potential interval. And these values consistently remained below 10 mΩ cm^2, indicating that platinum coatings endow surface-modified titanium bipolar plates with optimal improvement on conductivity and possess desirable durability applied in diverse PEMWE conditions.

4. Conclusion

In this work, electrochemical corrosion assessment techniques were

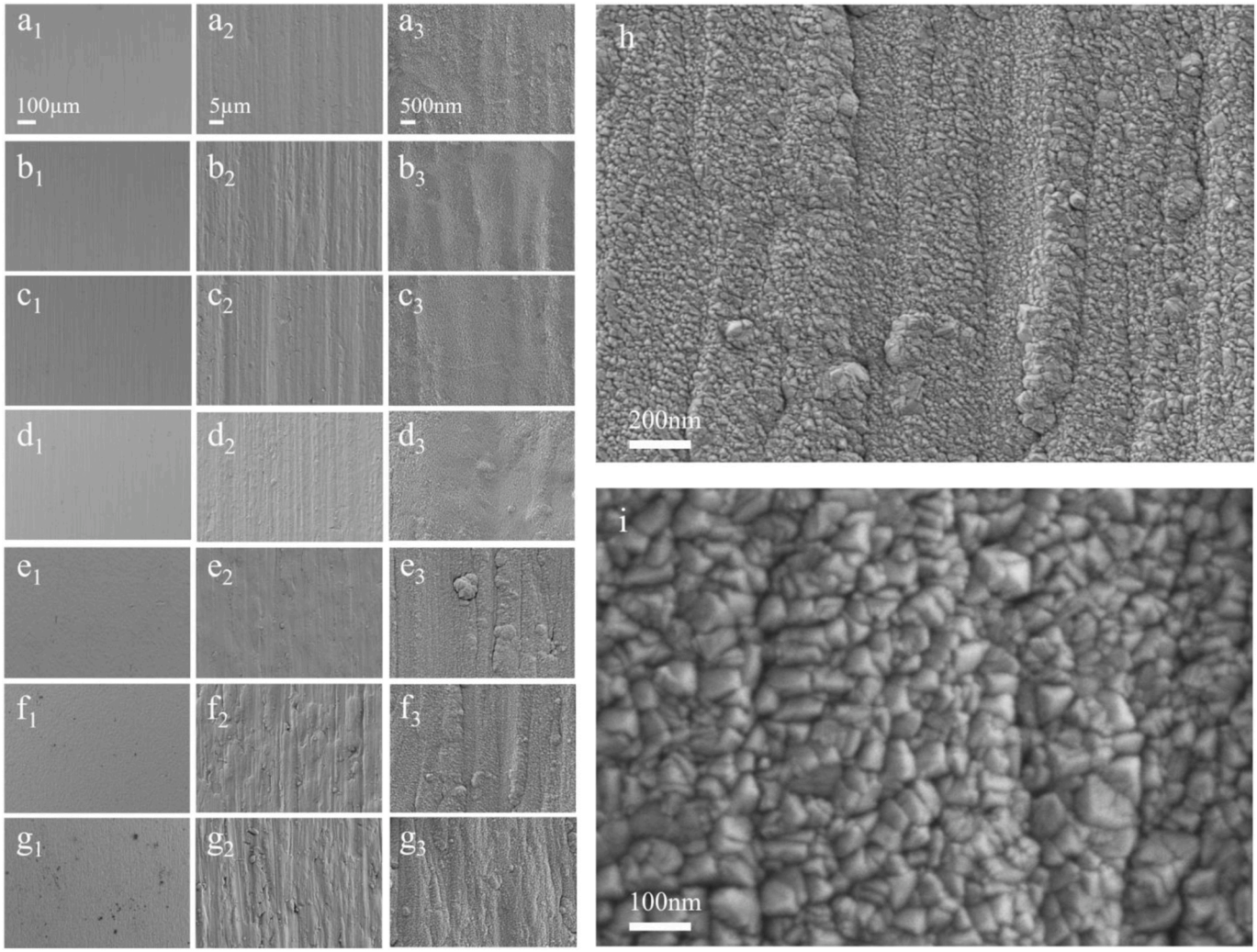

Fig. 10. SEM characterization of Pt/Ti samples surface after 10 h potentiostatic polarization in H_2SO_4 (pH = 3, 80 °C) (a_1-a_3) 0.6 $V_{Ag/AgCl}$ (b_1-b_3) 0.8 $V_{Ag/AgCl}$ (c_1-c_3) 1.0 $V_{Ag/AgCl}$ (d_1-d_3) 1.2 $V_{Ag/AgCl}$ (e_1-e_3) 1.4 $V_{Ag/AgCl}$ (f_1-f_3) 1.6 $V_{Ag/AgCl}$ (g_1-g_3) 1.8 $V_{Ag/AgCl}$ and (h,i) clustered particles after 10 h 1.8 $V_{Ag/AgCl}$ potentiostatic polarization.

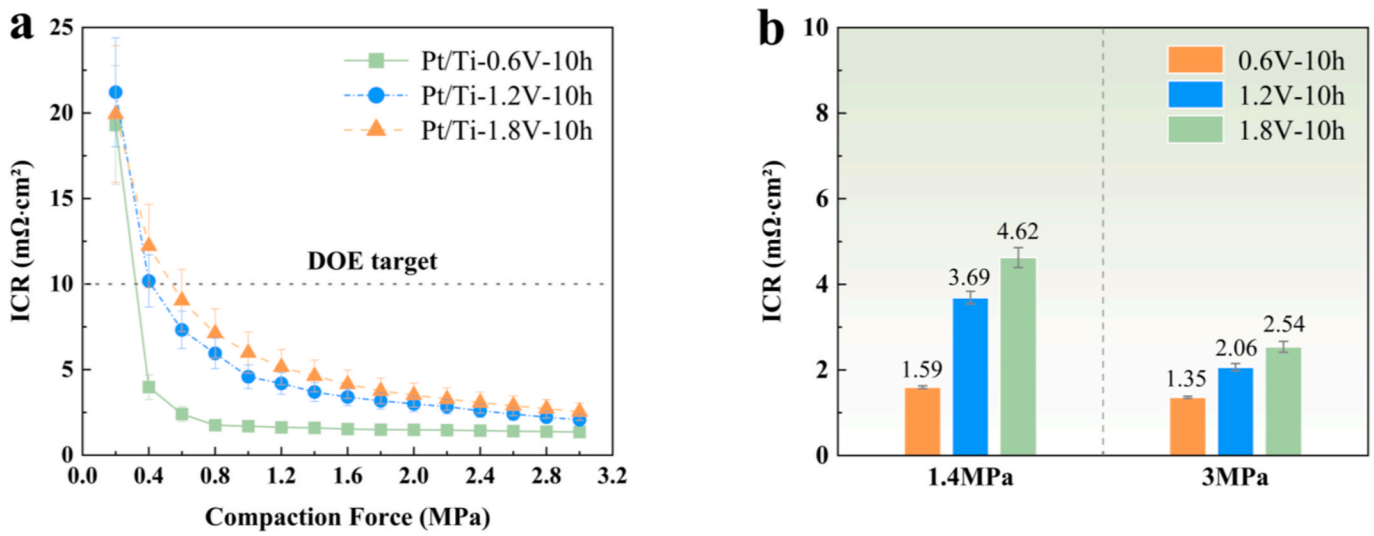

Fig. 11. (a) ICR of Pt/Ti samples with carbon papers after 10 h potentiostatic polarization in H_2SO_4 (pH = 3, 80 °C) with different applied potentials (b) comparison at 1.4 MPa and 3.0 MPa.

mainly employed to investigate the impact of diverse internal and external conditions in the electrolysis cell on the service performance of Pt/Ti bipolar plates. Our findings illustrate significant enhancements in both conductivity and corrosion resistance due to the platinum coating, thus promising improved efficiency and longevity of hydrogen production systems, yielding the following conclusions:

(1). Long-term tests further demonstrated that the coated plates maintained excellent conductivity in high voltage applications. Indicating that Pt coating can address the challenges posed by the non-conductive titanium dioxide layer traditionally observed in uncoated plates. Despite the promising results, the exact mechanisms by which environmental conditions affect the longevity of the coatings warrant further investigation to refine application protocols and maximize their performance.

(2). The interaction between environmental acidity and applied voltage significantly influenced corrosion behavior, indicating that the platinum coating could reduce corrosion particularly in more acidic settings. The corrosion current density observed at around 1.2 $V_{Ag/AgCl}$ showed a significant increase, accounting for its catalytic and corrosion-resistant performance. Therefore, the separation of bipolar plates corrosion resistance indicator formed from these two factors is required to realize a more accurate evaluation on surface modification choices.

CRediT authorship contribution statement

Yingyu Ding: Writing – original draft, Visualization, Methodology, Investigation, Formal analysis, Conceptualization. **Xiejing Luo:** Visualization, Resources, Data curation. **Luqi Chang:** Visualization, Resources, Investigation. **Xiang Li:** Writing – review & editing, Resources. **Wei Han:** Writing – review & editing, Methodology. **Chaofang Dong:** Writing – review & editing, Supervision, Project administration, Conceptualization.

Declaration of competing interest

The authors declare that they have no known competing financial interests or personal relationships that could have appeared to influence the work reported in this paper.

Acknowledgment

This work is supported by the National Natural Science Foundation of China (No. 52125102) and National Key R&D Program of China (No. 2021YFB4000100).

References

[1] Teuku H, Alshami I, Goh J, Masdar MS, Loh KS. Int J Energy Res 2021;45(15):20583–600.
[2] Wang Y, Diaz DFR, Chen KS, Wang Z, Adroher XC. Mater Today 2020;32:178–203.
[3] Miller HA, Bouzek K, Hnat J, Loos S, Bernaecker CI, Weissgaerber T, Roentzsch L, Meier-Haack J. Sustain Energy Fuels 2020;4(5):2114–33.
[4] Zhang J, Luo X, Ding Y, Chang L, Dong C. Int J Miner Metall Mater 2024;31(7):1599–616.
[5] Romero C, Benedetto D, Gordo E. Int J Hydrogen Energy 2024;52:1190–201.
[6] Huang L, Qi R. Int J Hydrogen Energy 2022;47(80):33903–18.
[7] Rojas N, Sanchez-Molina M, Sevilla G, Amores E, Almandoz E, Esparza J, Vivas MRC, Colominas C. Int J Hydrogen Energy 2021;46(51):25929–43.
[8] Meng Q, Yue X, Shang L, Liu X, Wang F, Zhang G. Int J Hydrogen Energy 2024;63:1105–15.
[9] Cheng H, Luo H, Wang X, Pan Z, Zhao Q, Dong C, Li X. Int J Hydrogen Energy 2023;48(98):38557–68.
[10] Luo X, Ren C, Song J, Luo H, Xiao K, Zhang D, Hao J, Deng Z, Dong C, Li X. J Mater Sci Technol 2023;146:19–41.
[11] Bazarah A, Majlan EH, Husaini T, Zainoodin AM, Alshami I, Goh J, Masdar MS. Int J Hydrogen Energy 2022;47(85):35976–89.
[12] Laedre S, Kongstein OE, Oedegaard A, Karoliussen H, Seland F. Int J Hydrogen Energy 2017;42(5):2713–23.
[13] Hala M, Malis J, Paidar M, Bouzek K. Membranes 2022;12(11).
[14] Lopes de Oliveira MC, Sayeg IJ, Ett G, Antunes RA. Int J Hydrogen Energy 2014;39(29):16405–18.
[15] Hu B, Chang FL, Xiang LY, He GJ, Cao XW, Yin XC. Int J Hydrogen Energy 2021;46(50):25666–76.
[16] Chen CY, Liang CH. Journal of the Chinese Society of Mechanical Engineers 2022;43(1):11–9.
[17] Hu Q, Gao JY, Shu S, Xu YX, Luo JL, Wang XZ. Corrosion Sci 2023;214.
[18] Chang L, Luo X, Ding Y, Zhang J, Gong X, Zhong Y, Yao J, Song J, Deng Z, Dong C. Thin Solid Films 2024;794:140294.
[19] Asri NF, Husaini T, Sulong AB, Majlan EH, Daud WRW. Int J Hydrogen Energy 2017;42(14):9135–48.
[20] Jin J, Liu H, Zheng D, Zhu Z. Int J Hydrogen Energy 2018;43(21):10048–60.
[21] McCay K, Laedre S, Martinsen SY, Smith G, Barnett AO, Fortin P. J Electrochem Soc 2021;168(6).
[22] Gaudig M, Muenchgesang W, Silva J, Pascher F, Hickmann T, Wehrspohn RB. Appl Phys Mater Sci Process 2023;129(2).
[23] Nam ND, Kim MJ, Jo DS, Kim JG, Yoon DH. Thin Solid Films 2013;545:380–4.
[24] Chanda UK, Behera A, Roy S, Pati S. Int J Hydrogen Energy 2018;43(52):23430–40.
[25] Mine EF, Ito Y, Teranishi Y, Sato M, Shimizu T. Int J Hydrogen Energy 2017;42(31):20224–9.
[26] Chen L, Liu R, Zhang B, Lv J, Zhang J. Mater Des 2022:224.
[27] Gao P, Xie Z, Ouyng C, Wu X, Lei T, Liu C, Huang Q. Micro & Nano Lett 2018;13(7):931–5.

[28] Bi J, Yang J, Liu X, Wang D, Yang Z, Liu G, Wang X. Int J Hydrogen Energy 2021;46(1):1144–54.
[29] Rikhari B, Mani SP, Rajendran N. RSC Adv 2016;6(83):80275–85.
[30] DOE Technical Targets for Polymer Electrolyte Membrane Fuel Cell Components. https://www.energy.gov/eere/fuelcells/doe-technical-targets-polymer-electrolyte-membrane-fuel-cell-components#bipolarplate.
[31] Sanchez-Molina M, Amores E, Rojas N, Kunowsky M. Int J Hydrogen Energy 2021;46(79):38983–91.
[32] Jung H-Y, Huang S-Y, Ganesan P, Popov BN. J Power Sources 2009;194(2):972–5.
[33] Ye H, Tu Z, Li S. J Power Sources 2024;595:234052.
[34] Li T, Zhang H, Wang Y, Wu C, Yan Y, Chen Y. Surf Coating Technol 2022;451.
[35] Ouyang C, Xun D. Coatings 2022;12(11).
[36] Abbas N, Qin X, Ali S, Zhu G, Yi Z, Yang X, Zeng X, Ullah Z, Gu K, Tang J. Int J Hydrogen Energy 2020;45(4):3186–92.
[37] Kumar AM, Ehsan MA, Suleiman RK, Murthy RVVR, Ahmed BA, Javid M. ACS Appl Energy Mater 2024;7(11):4879–90.
[38] Luo X, Chang L, Ren C, Zhang J, Zhang D, Yao J, Song J, Deng Z, Dong C, Li X. J Power Sources 2023;585.
[39] Liu G, Shan D, Fang B, Wang X. Int J Hydrogen Energy 2023;48(50):18996–9007.
[40] Wang Z, Zhang B, Gao K, Liu R. Int J Hydrogen Energy 2022;47(92):39215–24.
[41] Chen Y, Xu J, Xie ZH, Munroe P. Ceram Int 2022;48(13):19217–31.
[42] Tan Q, Wang Y. J Alloys Compd 2022;911.
[43] Peng S, Xu J, Xie ZH, Munroe P. Appl Surf Sci 2022;591.
[44] Meng W, Zhu H, Wang X, Li G, Fan Y, Sun D, Kong F. Metals 2022;12(5).
[45] Lin MT, Wan CH, Wu W. Thin Solid Films 2013;544:162–9.
[46] Liu G, Peng S, Hou F, Fang B, Wang X. Molecules 2022;27(19).
[47] Wang X, Luo H, Cheng H, Yue L, Deng Z, Yao J, Li X. Appl Energy 2024;357:122517.
[48] Zhang M, Hu L, Lin G, Shao Z. J Power Sources 2012;198:196–202.
[49] Zhang PC, Hao CM, Han YT, Du FM, Wang HY, Wang XY, Sun JC. Surf Coating Technol 2020;397.
[50] Feng S, Chen Q, Han X. J Electrochem Soc 2022;169(9).
[51] Meng Q, Yu L, Shang L, Wang F, Liu X, Zhang G. Diam Relat Mater 2023;135.
[52] Yan W, Zhang Y, Chen L, Luo J, Pang P, Zhang X, Liao B, Ying M. Diam Relat Mater 2021;120.
[53] Ding Y, Luo X, Chang L, Dong C. Electrochem Commun 2024;168.
[54] Yu L, Shang L, Zhang G, Li X, Meng Q. Int J Hydrogen Energy 2023;48(87):34055–66.
[55] Li H, Xin Y, Komatsu K, Guo P, Ma G, Ke P, Lee K-R, Saito H, Wang A. Int J Hydrogen Energy 2022;47(22):11622–32.
[56] Che J, Yi P, Peng L, Lai X. Int J Hydrogen Energy 2020;45(32):16277–86.
[57] Chen L, Liu R, Chen W, Zhang B, Lv J, Zhang J. Int J Hydrogen Energy 2024;58:326–32.
[58] Lim JW, Lee DG. Int J Hydrogen Energy 2013;38(28):12343–52.
[59] Jung HY, Huang SY, Popov BN. J Power Sources 2010;195(7):1950–6.
[60] Lettenmeier P, Wang R, Abouatallah R, Burggraf F, Gago A, Friedrich K. J Electrochem Soc 2016;163(11):F3119.
[61] Ren P, Pei P, Chen D, Zhang L, Li Y, Song X, Wang M, Wang H. Renew Energy 2022;194:1277–87.
[62] Salehmin MNI, Husaini T, Goh J, Sulong AB. Energy Convers Manag 2022;268:115985.
[63] Qiu D, Yi P, Peng L, Lai X. Int J Hydrogen Energy 2015;40(35):11559–68.
[64] Ma JJ, Xu J, Jiang S, Munroe P, Xie ZH. Ceram Int 2016;42(15):16833–51.
[65] Lædre S, Kongstein OE, Oedegaard A, Seland F, Karoliussen H. Int J Hydrogen Energy 2012;37(23):18537–46.
[66] Antunes RA, Oliveira MCL, Ett G, Ett V. Int J Hydrogen Energy 2010;35(8):3632–47.
[67] Davies D, Adcock P, Turpin M, Rowen S. J Power Sources 2000;86(1–2):237–42.
[68] Huang M, Tao J, Ma L, Zhuang X, Wang H, Bing Tao H, Zheng N. Chem Eng J 2024;498:155209.
[69] Bin S, Chen Z, Zhu Y, Zhang Y, Xia Y, Gong S, Zhang F, Shi L, Duan X, Sun Z. Int J Hydrogen Energy 2024;67:390–405.
[70] Wang H, Sweikart MA, Turner JA. J Power Sources 2003;115(2):243–51.
[71] Davies DP, Adcock PL, Turpin M, Rowen SJ. J Appl Electrochem 2000;30(1):101–5.
[72] Wang X, Luo H, Cheng H, Jin X, Song J, Li X. Chem Eng J 2024;483:149120.
[73] Furuya Y, Mashio T, Ohma A, Tian M, Kaveh F, Beauchemin D, Jerkiewicz G. ACS Catal 2015;5(4):2605–14.
[74] Gutić SJ, Dobrota AS, Fako E, Skorodumova NV, López N, Pašti IA. Catalysts 2020;10(3):290.
[75] Liu RT, Xu ZL, Li FM, Chen FY, Yu JY, Yan Y, Chen Y, Xia BY. Chem Soc Rev 2023;52(16):5652–83.